JASA Express Letters

SEPTEMBER 07 2022

# Difference between frequency and suppression tuning curves in a two-dimensional cochlear model

Yasuki Murakami; Takumi Fuji



*JASA Express Lett.* 2, 094402 (2022)
https://doi.org/10.1121/10.0013998

JASA EXPRESS LETTERS ARTICLE asa.scitation.org/journal/jel

# Difference between frequency and suppression tuning curves in a two-dimensional cochlear model

Yasuki Murakami[1,a)] and Takumi Fuji[2]
[1]Faculty of Design, Kyushu University, 4-9-1 Shiobaru, Minamiku, Fukuoka 815-8540, Japan
[2]Graduate School of Life Science and System Engineering, Kyushu Institute of Technology, 2-4 Hibikino, Wakamatsuku, Kitakyushu, Fukuoka 808-0135, Japan
murakami@design.kyushu-u.ac.jp, fuji.takumi792@mail.kyutech.jp

**Abstract:** Suppression tuning curves (STCs) can be used to evaluate the cochlear frequency selectivity. However, the tip of the STC is located at a higher frequency than that of the frequency tuning curve (FTC) measured in the same preparation. Therefore, this study compares STCs from one-dimensional (1D) and two-dimensional (2D) cochlear models, which ignore and include short waves, respectively. The simulated STC tip is at a higher frequency than that of FTC in the 2D model, unlike the 1D model. The result suggests that short waves in the 2D model are responsible for the upward frequency of STC relative to FTC. 

[Editor: Alessandro Altoè] https://doi.org/10.1121/10.0013998

**Received:** 14 July 2022 **Accepted:** 18 August 2022 **Published Online:** 7 September 2022

## 1. Introduction

The cochlea of the auditory system is responsible for extracting meaningful audio information based on the frequency of the incoming sound signals. The frequency tuning curve (FTC) identifies isolevel cochlear response to incoming sound at different frequency–intensity combinations and can evaluate the system's frequency selectivity. Direct measurement of responses on the basilar membrane (BM) in the cochlea produce typical FTCs exhibiting a single sharp tip at a characteristic frequency (CF) and an asymmetric shape (Rhode, 2007). Furthermore, auditory nerve (AN) firing matches these sharp, asymmetric properties (Narayan *et al.*, 1998). Moreover, considering the measurements of frequency selectivity in the case of humans, the forward auditory masking experiment shows quantitative similarities in the BM measurements and behavioral characteristics of the tuning curves (Oxenham and Shera, 2003).

Otoacoustic emissions (OAEs) provide a non-invasive objective assessment of frequency selectivity in human subjects. A pair of stimuli produces suppression effects in the cochlea, and a stimulus-frequency otoacoustic emission (SFOAE) is used to construct the suppression tuning curve (STC) (Keefe *et al.*, 2008). Based on quantitative similarities in the BM measurements and behavioral characteristics of the FTCs (Oxenham and Shera, 2003), two features of the SFOAE STC that differ from the BM FTC are (i) broader tuning at the tip frequency and (ii) an upward shift in frequency (Charaziak *et al.*, 2013). The broad tuning property suggests that the suppressive effects of the cochlea influence the STC results, which were obtained by comparing the simultaneously performed auditory masking experiments (Charaziak *et al.*, 2013). In addition, a different type of emission, such as the distortion product otoacoustic emission (DPOAE), generates STCs that are similar to those of SFOAEs in the same ears (Rasetshwane *et al.*, 2019). This implies that OAE STCs are independent of the emission type. Additionally, in the BM mechanical measurements performed on animals, a broad and upward frequency shift in STC has been observed (Dewey *et al.*, 2019). Thus, the STCs and FTCs obtained from the mechanical motion of the BM are significantly different. However, it is still unclear whether the mechanisms of the upward frequency shift of STC are different from those that produce the broadness of the STCs (Charaziak *et al.*, 2013). Although suppression occurs at the peak of the BM traveling wave when constructing the STCs, the broad spatial region before the peak affects the suppression as well (Geisler *et al.*, 1990; Versteegh and Heijden, 2013). These findings indicate that spatial effects of cochlear responses cause differences between the FTC and STC.

Modeling studies can be used to investigate the mechanisms of dynamical systems, such as the cochlear mechanical network. Using a cochlear model that includes two-degree-of-freedom (2DoF) micromechanics (Sisto *et al.*, 2019), Moleti and Sisto (2020) investigated the BM STC obtained from animal experiments (Dewey *et al.*, 2019). The results of the numerical simulations can reproduce the STCs in the micromechanical structure, such as the coupling between the

a)Author to whom correspondence should be addressed.

BM and reticular lamina (RL). However, the cochlear model did not reproduce the upward shift in frequency of the STC, that is, the tip frequency of the STC was consistent with that of the STC.

Moleti and Sisto (2020) performed numerical simulations using a one-dimensional (1D) cochlear model that approximates long-wave propagation and omits short waves. This simple 1D approximation with 2DoF models can reproduce the typical sharp tuning of mechanical BM motion via an active process (Neely and Kim, 1986). However, because two- and three-dimensional (2D and 3D) models approximate short-wave propagation, their behavior is naturally slightly different from that of 1D models. While many aspects of the long-wave approximation are consistent with observations, it has been suggested that the long-wave assumptions are inconsistent for many interesting frequencies and locations (Siebert, 1974). In addition, Watts (2000) reported that higher-order waves affect at the more apical site than the peak of the traveling wave. Indeed, it is necessary to include higher-order vibration modes into the analytical approximation to match the direct numerical solution (Watts, 2000; Elliott *et al.*, 2013). Therefore, the STC can be influenced by short-wave effects because a pair of stimuli generates two peaks of the BM wave traveling along the cochlear length.

This study investigates short fluid wave effects on the upward frequency shift of STC by comparing the 1D and 2D cochlear models. To compute the STC, we used the nonlinear 2DoF model proposed by Sisto *et al.* (2019). In Sec. 2, the 2D cochlear model used here is introduced, and the 1D model is derived from the 2D model with a set of boundary conditions. STCs are constructed from numerical simulations and compared with FTCs in Sec. 3. Finally, we discuss and conclude this paper in Sec. 4.

## 2. Model

The cochlea is a coiled duct divided by the BM into two chambers filled with fluid. The incoming sound via the stapes propagates from the base to the apex. In this process, the difference in fluid pressure across the BM induces BM motion. Moreover, the BM motion in turn influences the fluid pressure.

The present study considers an incompressible and non-viscous fluid flowing in a 2D plane. Solving the equation of motion and applying the mass conservation law for such a fluid, Neely (1981) derived the Laplace equation for the pressure difference between the two chambers $p$ as follows:

$$\frac{\partial^2 p(t)}{\partial x^2} + \frac{\partial^2 p(t)}{\partial y^2} = 0, \tag{1}$$

where $x$ and $y$ denote the distances from the stapes and the BM, respectively, and $t$ indicates the time series.

The boundary conditions to solve the Laplace equation were derived from the equation of motion for $x$ axis, which can be written as

$$\left.\frac{\partial p(t)}{\partial x}\right|_{x=0} = -2\rho\ddot{\xi}_s(t), \quad p(t)|_{x=L} = 0, \tag{2}$$

where $\ddot{\xi}_s$, $\rho$, and $L$ represent the acceleration of the stapes, fluid density, and cochlear length, respectively. Next, the boundary conditions for $y$ axis can be written as

$$\left.\frac{\partial p(t)}{\partial y}\right|_{y=0} = 2\rho\ddot{\xi}_1(t), \quad \left.\frac{\partial p(t)}{\partial y}\right|_{y=H} = 0, \tag{3}$$

where $\ddot{\xi}_1$ and $H$ represent acceleration of the BM and cochlear height, respectively.

To omit the short-wave effects of the cochlear fluid, we obtain a 1D model from the 2D fluid model in Eq. (1), with an approximation of the boundaries for $y$ axis in Eq. (3) as follows:

$$\frac{\partial^2 p(t)}{\partial x^2} - \frac{2\rho}{H}\ddot{\xi}_1(t) = 0. \tag{4}$$

We employed a 2DoF model of micro-cochlear mechanics with the 1D fluid model (Sisto *et al.*, 2019) in Eq. (4), which can account for the STC (Moleti and Sisto, 2020). The equation of motion of the 2DoF model can be written as

$$\begin{aligned} m_1\ddot{\xi}_1 + c_1\dot{\xi}_1 + k_1 xi_1 &= p - c_3(\dot{\xi}_1 - \dot{\xi}_2) - k_3(\xi_1 - \xi_2) + c_{nl}(\dot{\xi}_1 - \dot{\xi}_2) + k_{nl}(\xi_1 - \xi_2), \\ m_2\ddot{\xi}_2 + c_2\dot{\xi}_2 + k_2\xi_2 &= c_3(\dot{\xi}_1 - \dot{\xi}_2) + k_3(\xi_1 - \xi_2) - c_{nl}(\dot{\xi}_1 - \dot{\xi}_2) - k_{nl}(\xi_1 - \xi_2), \end{aligned} \tag{5}$$

where $m$, $c$ and $k$ represent the mass, resistance, and stiffness per area, respectively, and subscripts 1, 2, and 3 indicate the BM, RL, and gap between the BM and RL, respectively. Nonlinear coefficients $c_{nl}$ and $k_{nl}$ represent the feedback to the BM and RL, respectively, and can be written as

$$c_{nl}(\xi_1,\xi_2,\dot{\xi}_1,\dot{\xi}_2) = c_4\left(1-\tanh\left(\frac{(\xi_1-\xi_2)^2}{\xi_{sat}^2}+\frac{(\dot{\xi}_1-\dot{\xi}_2)^2}{\dot{\xi}_{sat}^2}\right)\right),$$
$$k_{nl}(\xi_1,\xi_2,\dot{\xi}_1,\dot{\xi}_2) = k_4\left(1-\tanh\left(\frac{(\xi_1-\xi_2)^2}{\xi_{sat}^2}+\frac{(\dot{\xi}_1-\dot{\xi}_2)^2}{\dot{\xi}_{sat}^2}\right)\right), \quad (6)$$

where $c_4$ and $k_4$ are the resistance and stiffness per unit area oriented from the feedback process, respectively.

In this study, we conducted numerical simulations to solve the cochlear problem using a fast Fourier transform-based solution in the time domain (Murakami, 2021). The same parameters for the 1D and 2D models used in the simulation were listed in the original study (Sisto *et al.*, 2019). The number of segments along the $x$ axis was set to 1500 for the 1D and 2D models. This value was selected because the calculation results diverge when the number of segments for $x$ axis is set below 1500 for the 2D model. Furthermore, depending on the number of segments along the $y$ axis for the 2D model, the degree of cochlear amplification caused by the action of $c_{nl}$ and $k_{nl}$ varies. Therefore, for the 2D model, the number of segments along the $y$ axis was set to 20 because the degree of cochlear amplification did not change when the value was set to over 20.

## 3. Results

### 3.1 Growth of suppression

The stimulus set consisted of a presentation of a sinusoid called the probe with frequency $f_p$ set to 4 kHz and a sinusoid called the suppressor with frequency $f_s$, which varied from 1 to 8 kHz (–2 to 1 octave re $f_p$). The intensity level of the probe $L_p$ was set to 30 dB. This is the level where the BM input–output function exhibits the nonlinear compressive property. The suppressor level $L_s$ was varied from 20 to 80 dB in steps of 10 dB. The stimulus duration was 150 ms. Recording began 50 ms after the stimulus was entered, which provides sufficient time to reach steady state.

The numerical simulation consisted of a BM velocity waveform $\dot{w}_1(x,t)$ along the cochlear length. Here, the BM velocity in response to the probe stimulus is $\dot{w}_1^p$, the suppressor stimulus is $\dot{w}_1^s$, and the simultaneous presentation of the probe and suppressor stimuli is $\dot{w}_1^{ps}$. The *residual* is defined as follows:

$$residual = \dot{w}_1^p(f_p) + \dot{w}_1^s(f_p) - \dot{w}_1^{ps}(f_p), \quad (7)$$

where, at the most sensitive position to the probe, $\dot{w}_1^p$, $\dot{w}_1^2$, and $\dot{w}_1^{ps}$ are defined as complex variables in the frequency domain using the fast Fourier transform. In the simulation, the length of the waveform was 100 ms, so the frequency resolution was 10 Hz.

Figure 1 shows the suppression residual curves for different suppressor frequencies in 1D and 2D models. For both models, the residual curves show steeper growth at the lower suppressor level $L_s$ and saturation at the higher suppressor level $L_s$. In particular, this trend was remarkable at $f_s$ = 4010 and 4590 for the 1D and 2D models, respectively. Furthermore, steeper growth occurs at higher $L_s$ for the lowest $f_s$. Moreover, the highest $f_s$ value generated a gentle slope for both models.

### 3.2 STC

We employed the decrement criterion (Keefe *et al.*, 2008; Rasetshwane *et al.*, 2019) to construct a STC. The suppression threshold was set at the suppression level $L_s$, where the residual level is 10.7 dB below the maximum value.

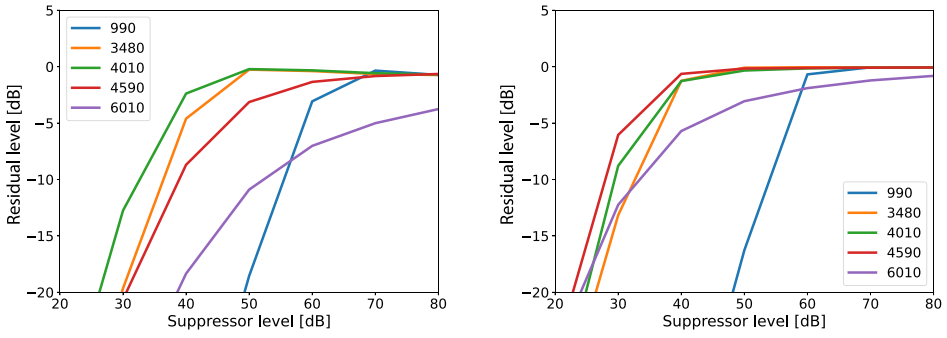


Fig. 1. Suppression residual as a function of the suppressor level with various suppressor frequencies.

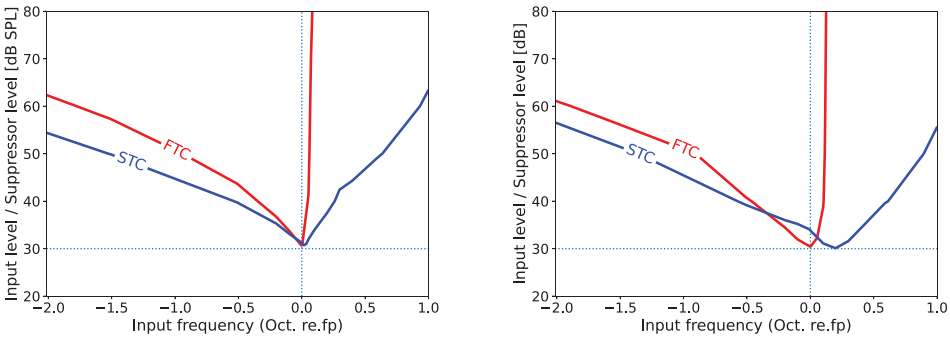


Fig. 2. STCs (blue) compared with FTCs (red).

Figure 2 compares STCs and FTCs. The STCs indicate broader tuning than FTCs for both models. In particular, the slope of the STCs is gentler on the high-frequency side than that of the FTCs. For the 1D model, the tip frequency of the STC was similar to that of the FTC. However, the STC's tip frequency was higher than that of FTC.

### *3.3 STC metrics*

For FTC and STC, the high-frequency slope, cochlear amplifier gain, tuning frequency, and amount of tuning were calculated to evaluate its shape quantitatively, following a previous study on SFOAE STC (Rasetshwane *et al.*, 2019). The high-frequency slope is estimated to be the STC slope over the segment where the suppressor frequency $f_s$ is larger than the tip frequency. The cochlear amplifier gain estimate is defined as the tip-to-tail difference. The tail of the STC is defined as the suppression threshold, where the suppressor frequency $f_s$ was set to 990 Hz (–2 octaves re $f_p$). The tip is defined as the minimum of the STC. The amount of tuning was estimated using $Q_{ERB}$, which is defined as the probe frequency $f_p$ divided by the equivalent rectangular bandwidth (ERB) (Shera *et al.*, 2010).

Table 1 compares the tuning properties of different types of curves and modeling dimensions.

### *3.4 Spatial distribution of responses*

As shown in Fig. 2, the simulated STCs exhibited the spatial-dimension effects in the models developed considering the tip-frequency shifting. This result indicates that the short wave effect led to the tip frequency shift because the 1D and 2D models ignore and include short waves, respectively. Now, we observe short-wave effects in the BM velocity and pressure difference affecting the BM under the condition for obtaining the tip shaping of the STCs, as shown in Fig. 3. The BM velocity distribution depends on the modeling dimensions. However, the phase of the BM velocity is not affected by the suppressor. In both models, the phase indicates that the pressure wave propagates from the base to the apex. However, the amplitude distributions differ between the two models.

## 4. Discussion

The present study investigated unique STC properties, such as broad tuning and upward frequency shifting, using a 2D cochlear model. A previous modeling study conducted by Moleti and Sisto (2020) could not reproduce the upward frequency shift of STCs using a 1D cochlear model including 2DoF micromechanics (Sisto *et al.*, 2019). However, they could satisfactorily account for STCs in the micromechanical structure on the BM with the numerical simulation applying the long-wave assumption.

The 2D cochlear model could reproduce unique properties, such as broad tuning and upward frequency shift in STC compared with FTC, as shown in Fig. 2(b). As illustrated in Fig. 2(a), the 1D cochlear model exhibited a broader STC than FTC; however, the tip frequency was consistent between the STC and FTC. Thus, despite using the same 2DoF micromechanical model, the numerical results indicate that the upward frequency shift depends on the dimensions of the

Table 1. Tuning curve metrics.

| Tuning curve parameter | FTC-1D | FTC-2D | STC-1D | STC-2D |
|---|---|---|---|---|
| High-frequency slope (dB/octave) | 586 | 382 | 33.5 | 32.1 |
| Tip-to-tail difference (dB) | 31.6 | 30.7 | 23.6 | 26.3 |
| Tip frequency (octave) | 0.00 | 0.00 | 0.02 | 0.20 |
| $Q_{ERB}$ | 16.6 | 15.7 | 8.0 | 6.7 |

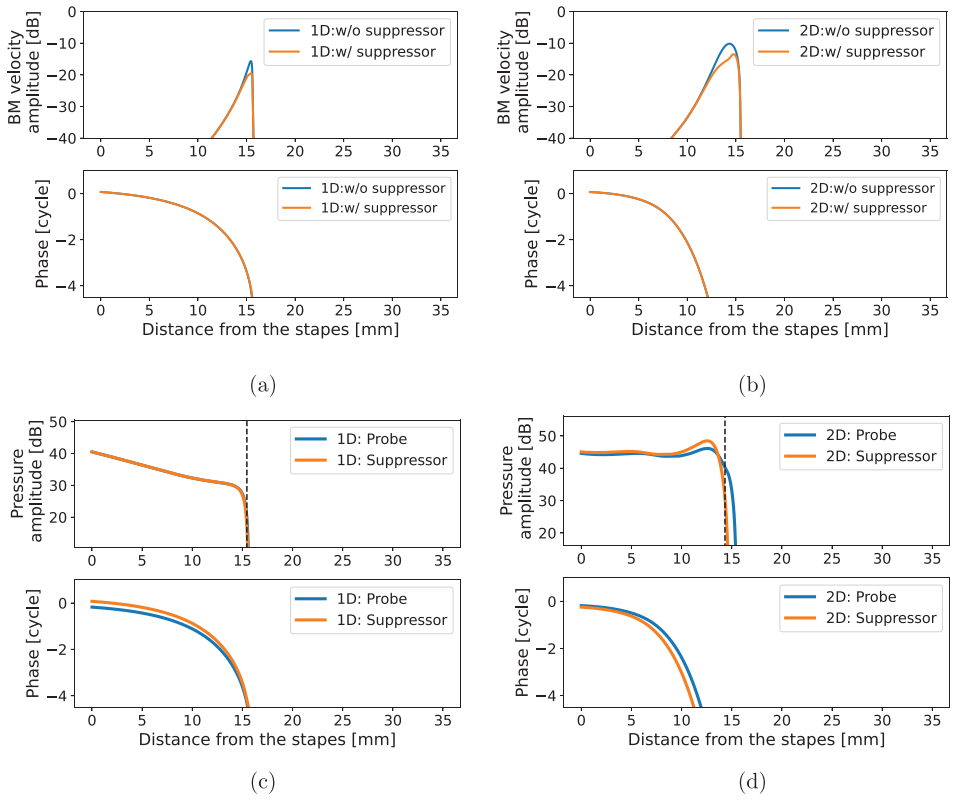


Fig. 3. (a) and (b) BM velocity for the probe along the cochlear length. (c) and (d) Pressure difference affecting the BM with introduction of the probe and the suppressor. The frequencies of the suppressors $f_s$ and $L_s$ were set to 4050 and 4590 Hz for the 1D and the 2D models at 30 dB, respectively. Those values denote the tip of the STCs in Fig. 2. Dashed lines represent the CF site for the probe.

model. The tuning curve metrics highlight this feature, as listed in Table 1. In the STC obtained from the 2D model, the tip frequency rose by 0.20 octave compared to the probe frequency. This value is consistent with the measurements of cochlear motion (Dewey *et al.*, 2019) and OAEs (Rasetshwane *et al.*, 2019). The values of the high-frequency slope, tip-to-tail difference, and asymmetry in the STCs decreased compared with FTCs. Furthermore, the values of $Q_{ERB}$ indicate broader tuning of STCs, consistent with OAEs and auditory masking experiments (Rasetshwane *et al.*, 2019; Oxenham and Shera, 2003).

The 1D and 2D models neglect and include the short wave in the pressure difference propagation, respectively. Figure 3 shows that BM and pressure difference are affected by short-waves dynamics. As shown in Fig. 3, the suppressor reduced the amplitudes of the BM velocity for the 1D and 2D model around the CF site. Remarkably, the peak position of the BM traveling wave was moved toward the apex when the suppressor was presented for the 2D model. Thus, this result implies that the suppressor shifts the tip of the tuning curve properties toward higher frequency. Using a wave finite element analysis for a passive cochlear model, Elliott *et al.* (2013) pointed out that higher-order waves significantly contribute beyond the CF site. As shown in Fig. 3, our numerical results confirm that the dimensional differences are influential before the CF site. The difference between our numerical simulation and the analysis by Elliott *et al.* (2013) can be attributed to the fact that this study focused on short-wave dynamics, whereas Elliott *et al.* (2013) analyzed higher-order waves. Moreover, Altoè *et al.* (2021) reported that the amplitude of the BM response depends primarily on the nonlinear properties of the traveling wave in more basal (high-frequency) regions near the peak of the traveling wave. Similarly, Fig. 3 showed that the suppressor affected the spatial pattern of the BM velocity and pressure in more basal regions to the peak of the traveling wave, forming more complex patterns in the 2D model compared to the 1D model.

In this study, a 2D cochlear model, including the 2DoF micromechanical model, successfully reproduced the upward frequency shift in the STC. By comparing the results obtained from 1D and 2D models, we conclude that short waves affect this phenomenon. Notably, the suppressor moved the peak of the spatial distribution of the BM response toward the apical region for the 2D model. Therefore, we concluded that the short-wave effect affects the CF site's variability and shifts the STC's tip at a higher frequency than that of the FTC.

**Acknowledgment**

This work was supported by Japan Society for the Promotion of Science (JSPS) KAKENHI Grant No. 21K17765.

## References and links


Altoè, A., Charaziak, K. K., Dewey, J. B., Moleti, A., Sisto, R., Oghalai, J. S., and Shera, C. A. (**2021**). "The elusive cochlear filter: Wave origin of cochlear cross-frequency masking," J. Assoc. Res. Otolaryngol. **22**, 623–640.

Charaziak, K. K., Souza, P., and Siegel, J. H. (**2013**). "Stimulus-frequency otoacoustic emission suppression tuning in humans: Comparison to behavioral tuning," J. Assoc. Res. Otolaryngol. **14**, 843–862.

Dewey, J. B., Applegate, B. E., and Oghalai, J. S. (**2019**). "Amplification and suppression of traveling waves along the mouse organ of corti: Evidence for spatial variation in the longitudinal coupling of outer hair cell-generated forces," J. Neurosci. **39**, 1805–1816.

Elliott, S. J., Ni, G., Mace, B. R., and Lineton, B. (**2013**). "A wave finite element analysis of the passive cochlea," J. Acoust. Soc. Am. **133**, 1535–1545.

Geisler, C. D., Yates, G. K., Patuzzi, R. B., and Johnstone, B. M. (**1990**). "Saturation of outer hair cell receptor currents causes two-tone suppression," Hear. Res. **44**, 241–256.

Keefe, D. H., Ellison, J. C., Fitzpatrick, D. F., and Gorga, M. P. (**2008**). "Two-tone suppression of stimulus frequency otoacoustic emissions," J. Acoust. Soc. Am. **123**, 1479–1494.

Moleti, A., and Sisto, R. (**2020**). "Suppression tuning curves in a two-degrees-of-freedom nonlinear cochlear model," J. Acoust. Soc. Am. **148**(1), EL8–EL13.

Murakami, Y. (**2021**). "Fast time-domain solution of a nonlinear three-dimensional cochlear model using the fast Fourier transform," J. Acoust. Soc. Am. **150**, 2589–2599.

Narayan, S. S., Temchin, A. N., Recio, A., and Ruggero, M. A. (**1998**). "Frequency tuning of basilar membrane and auditory nerve fibers in the same cochleae," Science **282**, 1882–1884.

Neely, S. T. (**1981**). "Finite difference solution of a two-dimensional mathematical model of the cochlea," J. Acoust. Soc. Am. **69**, 1386–1391.

Neely, S. T., and Kim, D. (**1986**). "A model for active elements in cochlear biomechanics," J. Acoust. Soc. Am. **79**, 1472–1480.

Oxenham, A. J., and Shera, C. A. (**2003**). "Estimates of human cochlear tuning at low levels using forward and simultaneous masking," J. Assoc. Res. Otolaryngol. **4**, 541–554.

Rasetshwane, D. M., Bosen, E. C., Kopun, J. G., and Neely, S. T. (**2019**). "Comparison of distortion-product otoacoustic emission and stimulus-frequency otoacoustic emission two-tone suppression in humans," J. Acoust. Soc. Am. **146**, 4481–4492.

Rhode, W. S. (**2007**). "Basilar membrane mechanics in the 6–9 kHz region of sensitive chinchilla cochleae," J. Acoust. Soc. Am. **121**, 2792–2804.

Shera, C., Guinan, J. J., and Oxenham, A. J. (**2010**). "Otoacoustic estimation of cochlear tuning: Validation in the chinchilla," J. Assoc. Res. Otolaryngol. **11**, 343–365.

Siebert, W. M. (**1974**). "Ranke revisited—A simple short-wave cochlear model," J. Acoust. Soc. Am. **56**, 594–600.

Sisto, R., Shera, C. A., Altoè, A., and Moleti, A. (**2019**). "Constraints imposed by zero-crossing invariance on cochlear models with two mechanical degrees of freedom," J. Acoust. Soc. Am. **146**, 1685–1695.

Versteegh, C. P. C., and Heijden, M. V. D. (**2013**). "The spatial buildup of compression and suppression in the mammalian cochlea," J. Assoc. Res. Otolaryngol. **14**, 523–545.

Watts, L. (**2000**). "The mode-coupling Liouville–Green approximation for a two-dimensional cochlear model," J. Acoust. Soc. Am. **108**, 2266–2271.